MATHEMATICAL BIOSCIENCES
AND ENGINEERING
Volume **3**, Number **2**, April **2006**

http://www.mbejournal.org/

pp. **371–383**

SIMULATION OF PULSATILE FLOW OF BLOOD IN STENOSED CORONARY ARTERY BYPASS WITH GRAFT

B. Wiwatanapataphee

Department of Mathematics, Mahidol University
Payathai, Bangkok, Thailand 10400

D. Poltem

Department of Mathematics, Mahidol University
Payathai, Bangkok, Thailand 10400

Y.H. Wu

Department of Mathematics and Statistics, Curtin University of Technology
GPO Box U1987, Perth 6845, Western Australia

Y. Lenbury

Department of Mathematics, Mahidol University
Payathai, Bangkok, Thailand 10400

(Communicated by Yang Kuang)

Abstract. In this paper, we investigate the behavior of the pulsatile blood flow in a stenosed right coronary artery with a bypass graft. The human blood is assumed to be a non-Newtonian fluid and its viscous behavior is described by the Carreau model. The transient phenomena of blood flow though the stenosed region and the bypass grafts are simulated by solving the three dimensional unsteady Navier-Stokes equations and continuity equation. The influence of the bypass angle on the flow interaction between the jet flow from the native artery and the flow from the bypass graft is investigated. Distributions of velocity, pressure and wall shear stresses are determined under various conditions. The results show that blood pressure in the stenosed artery drops dramatically in the stenosis area and that high wall shear stresses occur around the stenosis site.

1. **Introduction.** Cardiovascular disease has been one of the major causes of death in developed countries [1]. Most of the cases are associated with some form of abnormal blood flow in arteries, which is induced by the existence of stenoses [2, 3, 4]. At the neck of a stenosis, the local pressure reduces because of the acceleration of the flow through the narrowing section. When the degree of stenosis is very high, the pressure may be lower than the external pressure at the neck of the stenosis, and consequently the stenosis may collapse, causing choking of the flow and likely leading to heart attack [5].

In recent years, surgical treatments of cardiovascular diseases have been developed rapidly, and coronary artery bypass grafting (CABG) has been widely used for patients with severe coronary artery diseases [2, 6]. Different kinds and shapes

2000 *Mathematics Subject Classification.* 92C10.

Key words and phrases. mathematical modelling, blood flow, stenosis, coronary artery, bypass graft.

of bypass anastomoses are available at present, and consequently different surgery procedures are used to set up a bypass. However, up to 25% of the grafts become occluded within one year and up to 50% occluded within ten years [7]. To reduce the surgical and post-surgical failures, it is thus essential to further study the flow behavior of blood through the bypass graft. Mathematical modelling of physiological flows will lead to a better understanding of the phenomena involved in coronary artery diseases [9, 10]. This will not only reduce the number of bypass graft failures, but also may suggest new methods in bypass surgical procedures.

The flow in the coronary artery with a bypass graft was studied by numerous authors [2, 6, 8, 12, 17, 18, 19]. In these studies, blood was modeled as a Newtonian fluid. The viscoelasticity of blood was ignored under the assumption that the shear rate is larger than 100 s^{-1}. In the last two decades, many researchers [3, 14, 15, 16, 20] numerically investigated the influence of the non-Newtonian properties of blood on the flow in three-dimensional coronary artery models. All of the above studies investigated blood flow based on some assumptions, for instance, constant velocity at the inlet and constant pressure at the outlet. The use of constant pressure at the outlet may introduce unrealistic artificial wave-reflections. Also, until recently, none of the studies concentrated on the influence of the bypass graft angle using a non-Newtonian model on the flow patterns and the wall shear stress in the artery.

In this study, we simulated the unsteady non-Newtonian blood flow in the 75% stenosed right coronary artery. The three-dimensional Navier-Stokes equations coupled with a non-Newtonian model are solved numerically using the Galerkin finite element method. The effect of using different bypass graft angles, 45°, 60° and 90°, on the flow pattern is investigated.

2. **Mathematical Model.** Precise analysis of blood flow through arteries requires coupling of the blood flow with the elastic deformation of the blood vessel. In this work, to capture the main feature of blood flow through stenotic arteries with a bypass graft and to keep the model simple, the effect of the deformation of blood vessels on blood flow is neglected. It has been generally accepted that human blood behaves as a Newtonian fluid when the shear rate is greater than 100 s^{-1}. However, when the shear rate is lower than 100 s^{-1}, blood behaves as a non-Newtonian fluid, and the shear stresses depend nonlinearly on the deformation rate [21]. In pulsatile blood flow, the instantaneous shear rate over a cardiac cycle may vary from zero to more than 1000 s^{-1} depending on the problem under examination, as shown in section 4 of this paper. Therefore, in this study, human blood is modelled as a non-Newtonian fluid, and the stress-deformation rate relation is described by

$$\sigma = -pI + 2\eta(\dot{\gamma})\mathbf{D}, \tag{1}$$

where p is the pressure and D is the rate of deformation tensor given by

$$\mathbf{D} = \frac{1}{2}\left(\nabla\mathbf{u} + (\nabla\mathbf{u})^T\right);$$

η and $\dot{\gamma}$ denote respectively the viscosity of blood and shear rate. Various non-Newtonian models have been proposed to describe the relation between η and $\dot{\gamma}$. In this work, we use Carreau's shear-thinning model, namely,

$$\eta = \eta_\infty + (\eta_0 - \eta_\infty)\left[1 + (\lambda\dot{\gamma})^2\right]^{(n-1)/2},$$

in which $\dot{\gamma} = \sqrt{2tr(\mathbf{D}^2)}$ is a scalar measure of the rate of deformation tensor, and η_0 and η_∞ denote the zero shear viscosity and the infinite shear viscosity. The

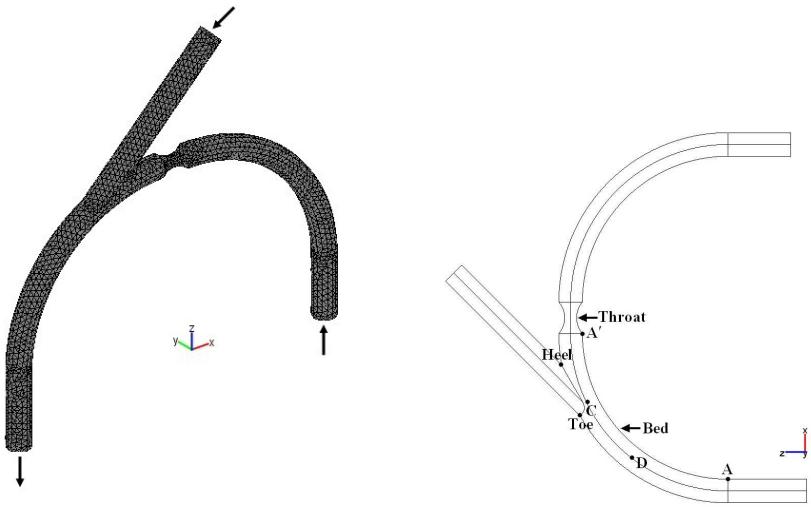

(a) (b)

FIGURE 1. Geometry of the three-dimensional 75% stenosed right coronary artery with bypass grafting model: (a) global view, (b) x-z view.

consistency index, n, is a parameter whose value is between 0 and 1. Based on Cho and Kensey [11], the parameters have the following typical values: $\eta_\infty = 0.0345\ \mathrm{g\,cm^{-1}\,s^{-1}}$, $\eta_0 = 0.56\ \mathrm{g\,cm^{-1}\,s^{-1}}$, $n = 0.3568$, and $\lambda = 3.313\,\mathrm{s}$.

The equations governing the blood flow include the constitutive equation (1) and the following continuity and stress equations of motion:

$$\nabla \cdot \mathbf{u} = 0, \tag{2}$$

$$\frac{\partial \mathbf{u}}{\partial t} + \mathbf{u} \cdot \nabla \mathbf{u} = \frac{1}{\rho} \nabla \cdot \sigma, \tag{3}$$

where ρ denotes the blood density.

By substituting equation (1) into (3), we have the following Navier-Stokes equations

$$\frac{\partial \mathbf{u}}{\partial t} + \mathbf{u} \cdot \nabla \mathbf{u} = \frac{1}{\rho} \nabla \cdot [-pI + \eta(\nabla \mathbf{u} + (\nabla \mathbf{u})^T)]. \tag{4}$$

To completely define the flow problem, boundary conditions for the velocity and pressure fields must be specified. For a typical coronary artery bypass grafting system, the boundary of the computation region consists of four parts, namely, the inflow surface of the native artery and the bypass graft, the artery wall, and the outflow boundary.

On the inflow surfaces, the velocity is set to the pulsatile velocity $\bar{u}_{in}(t) = Q(t)/A$, where A is the cross-section area of the inlet surface [cm^2] and $Q(t)$ is the pulsatile flow rate [ml/s], as shown in Figure 2 [12]. First, a spatially averaged mean velocity is used on the inlet boundary. With the use of the no-slip condition on the arterial wall, a parabolic velocity profile develops at a small distance from the inlet boundary, which is then used for the inflow boundary condition. The flow

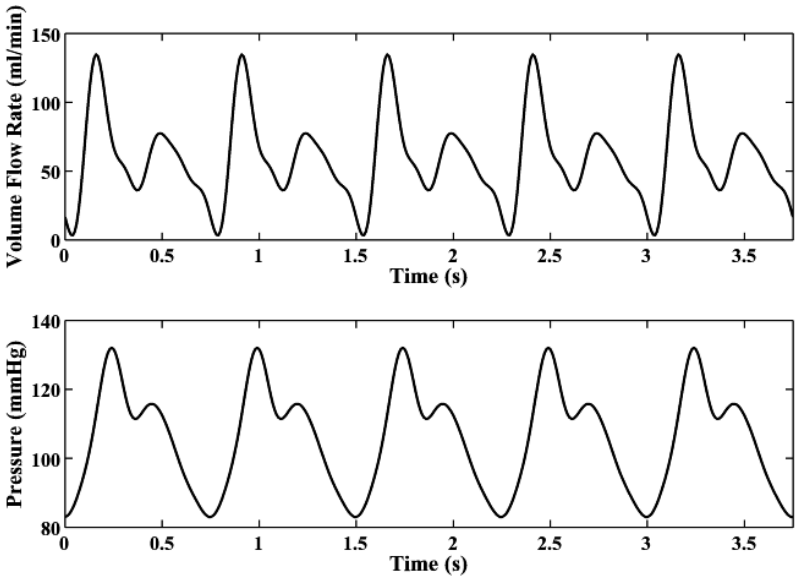

FIGURE 2. The blood volume flow rate and pressure in the right coronary artery.

waveform can be written in the form of the following Fourier series:

$$Q(t) = \overline{Q} + \sum_{n=1}^{5} Q_n cos(n\omega t - \alpha_n), \tag{5}$$

where $\bar{Q}$ is the mean volume flow rate, and $\omega = \dfrac{2\pi}{T}$ is the angular frequency with period $T = 0.75$s. The no-slip condition is applied to the artery wall. On the outflow boundary, the normal stress is specified; that is,

$$\sigma \cdot \mathbf{n} = -p(t)\mathbf{n},$$

where $\mathbf{n}$ is the unit normal vector to the outlet section. We assume the pressure at the outlet to be the pulse pressure as shown in Figure 2. The pulsatile pressure takes the form of the following Fourier series:

$$p(t) = \overline{p} + \sum_{n=1}^{5} p_n cos(n\omega t - \beta_n), \tag{6}$$

where $\bar{p}$ is the mean pressure.

In summary, the fluid flow problem in the coronary artery bypass grafting is governed by the following boundary value problem.

BVP: Find $\mathbf{u}$ and p such that the field equations (2) and (4) are satisfied in Ω and all boundary conditions are satisfied.

3. **A Numerical Algorithm Based on the Finite Element Method.** To develop a variational statement corresponding to the BVP, we consider the following alternative problem:

Find $\mathbf{u}$ and $p \in H^1(\Omega)$ such that for all $\mathbf{w}^u$ and $w^p \in H_0^1(\Omega)$, all boundary conditions are satisfied and

$$\begin{gathered}(\nabla \cdot \mathbf{u}, w^p) = 0, \\ \left(\frac{\partial \mathbf{u}}{\partial t}, \mathbf{w}^u\right) + (\mathbf{u} \cdot \nabla \mathbf{u}, \mathbf{w}^u) = \frac{1}{\rho}\left(\nabla \cdot [-pI + \eta(\nabla \mathbf{u} + (\nabla \mathbf{u})^T)], \mathbf{w}^u\right),\end{gathered} \tag{7}$$

where $(\cdot, \cdot)$ denotes the inner product on the square integrable function space, and $L^2(\Omega), H^1(\Omega)$ is the Sobolev space $W^{1,2}(\Omega)$ with norm $\| \cdot \|_{1,2,\Omega}$ and $H_0^1(\Omega) = \{v \in H^1(\Omega) | v = 0$ on the Dirichlet type boundary$\}$.

To find the Galerkin numerical solution of the above problem, we pose the problem into a finite dimension subspace. Firstly, we choose an N-dimensional subspace $H_h \subset H^1(\Omega)$ for $\mathbf{u}$ and the corresponding test function. Let $\{\phi_i\}_{i=1}^N$ be the basis functions of H_h; then we have

$$\mathbf{u}(\mathbf{x}, t) \approx (\mathbf{u})_h = \sum_{i=1}^{N} \phi_i(\mathbf{x}) \mathbf{u}_i(t), \tag{8}$$

$$\mathbf{w}^u \approx (\mathbf{w}^u)_h = \sum_{i=1}^{N} \phi_i(\mathbf{x}) \mathbf{w}_i^u(t). \tag{9}$$

Secondly, we choose an M-dimensional subspace $H_\beta \subset H^1(\Omega)$ for p and w^p. Let $\{\psi_i\}_{i=1}^M$ be the basis functions of H_β; then we have

$$p(\mathbf{x}, t) \approx p_h = \sum_{i=1}^{M} \psi_i(\mathbf{x}) p_i(t), \tag{10}$$

$$w^p \approx (w^p)_h = \sum_{i=1}^{M} \psi_i(\mathbf{x}) w_i^p(t). \tag{11}$$

In principle, H_β can be chosen to be the same as H_h. However, our numerical experiments have shown that it is necessary to choose H_β to be different from H_h to ensure the convergence of the solution to the problem.

By substituting (8)-(11) into (7), noting that $\mathbf{w}^u$ and w^p are arbitrary and using Green's formula, we have

$$\int_\Omega \Psi \frac{\partial \Phi^T}{\partial x_i} d\Omega \mathbf{U}_i = 0, \tag{12}$$

$$\begin{aligned}&\int_\Omega \Phi \Phi^T d\Omega \frac{\partial \mathbf{U}_i}{\partial t} + \int_\Omega \Phi u_j \frac{\partial \Phi^T}{\partial x_j} d\Omega \mathbf{U_i} - \frac{1}{\rho} \int_\Omega \frac{\partial \Phi}{\partial x_i} \Psi^T d\Omega P \\ &\quad + \frac{1}{\rho} \int_\Omega \eta \frac{\partial \Phi}{\partial x_j} \frac{\partial \Phi^T}{\partial x_j} d\Omega \mathbf{U_i} + \frac{1}{\rho} \int_\Omega \eta \frac{\partial \Phi}{\partial x_j} \frac{\partial \Phi^T}{\partial x_i} d\Omega \mathbf{U_j} + \frac{1}{\rho} \int_{\Gamma_{exit}} \Phi \Psi \, d\Gamma P = 0,\end{aligned} \tag{13}$$

where $\Psi = (\psi_1, \psi_2, \ldots, \psi_N)^T$, $\Phi = (\phi_1, \phi_2, \ldots, \phi_N)^T$, and $\mathbf{U}_i = (u_{1i}, u_{2i}, \ldots, u_{Ni})$.

The system (12)-(13) can be combined and written in matrix form as follows:

$$\begin{aligned}C^T U &= 0, \\ M\dot{U} + A(U)U + \overline{C}P &= F.\end{aligned} \tag{14}$$

Using the backward Euler differentiation scheme for a typical time step ($t_n \to t_{n+1}$), we have

$$\begin{aligned} C^T U_{n+1} &= 0, \\ \left(\frac{M}{\Delta t_n} + A\right) U_{n+1} + \overline{C} P_{n+1} &= F_{n+1} + \frac{M}{\Delta t_n} U_n, \end{aligned} \tag{15}$$

which is nonlinear because A depends on U_{n+1}. To deal with this nonlinearity for an iterative solution of (15), we use the following iterative updating:

$$\begin{aligned} C^T U_{n+1}^{i+1} &= 0, \\ \left(\frac{M}{\Delta t_n} + A_{n+1}^i\right) U_{n+1}^{i+1} + \overline{C} P_{n+1}^{i+1} &= F_{n+1}^i + \frac{M}{\Delta t_n} U_n^i, \end{aligned} \tag{16}$$

where the superscript i denotes evaluation at the ith iteration step. Therefore, in a typical time step ($t_n \to t_{n+1}$), starting with $U_{n+1}^0 = U_n$, we determine U_{n+1}^{i+1} and P_{n+1}^{i+1} by solving system (16) repeatedly until $\left\|U_{n+1}^{i+1} - U_{n+1}^i\right\| < \varepsilon_u$ and $\left\|P_{n+1}^{i+1} - P_{n+1}^i\right\| < \varepsilon_p$.

By repeatedly using the above procedure for $n = 0, 1, 2, \ldots$ we can determine the state U and P of the system at $t_0, t_1, t_2, \ldots$. If the norm $\|U_{n+1} - U_n\|$ and $\|P_{n+1} - P_n\|$ are sufficiently small, then the system approaches the so-called steady state.

4. **Numerical Results.** Flow simulations were conducted under a typical physiological condition. The fluid properties are typical of human blood with a density of 1.06 gcm^{-3} [5]. The computation region, as shown in Figure 1, represents the right coronary artery with a 75 % stenosis located at 3.95 cm from the inlet boundary. The diameter of the native artery is equal to 0.3 cm (D), and the diameter of the graft is equal to $0.96 \times D$ cm[13]. The length of the artery is 8.5 cm for a typical coronary artery in this investigation. It should be noted that we have used an idealized geometry here in our model. For a real blood vessel, the cross-section is not perfectly circular, and the cross-section area also varies along the axial position. This simplification indicates that some arteries may have a larger risk of restenosis than others. The values of Q_n, α_n in (5) and p_n and β_n in (6) are given in Table 1. The mean flow rate ($\bar{Q}$) and mean pressure ($\bar{p}$) are equal to 59.09 ml/min and 122.5 mmHg, respectively.

We simulate the three-dimensional blood flow through the stenosed right coronary artery with the 45°, 60°, and 90° bypass operations. The mesh as shown in Figure 1 consists of 15,819 tetrahedral elements with 27,030 nodes corresponding to 85,068 degrees of freedom. To get the transient flow patterns in cardiac cycles, each cycle is divided into 1,051 time steps with step size of 3.57 ms.

Figure 3 shows the velocity profile of blood flow in the right coronary artery with a 45° bypass graft. It clearly outlines how the flow goes through the stenosed artery.

TABLE 1. The parameter values used in the computation.

n	Q_n	α_n	p_n	β_n
1	17.28	-4.027	-21.740	-0.406
2	-34.91	-6.509	-9.088	0.202
3	16.11	-1.913	4.771	-0.633
4	11.70	-1.461	2.035	-4.315
5	6.64	-0.074	0.768	3.932

The velocity at the stenosis region suddenly tends to decrease at the downstream when we use the bypass operation.

Figures 4 shows the vector plot and the streamline plot of the blood flow on the x-z plane in the stenosed right coronary artery with no and with 45°, 60°, and 90° angles of bypass graft. The maximum blood velocity at the throat of stenosis decreases to 113.2, 90.57, 111.3, and 113.1 cm/s at the downstream, point C, for the geometry with no bypass graft and with 45°, 60°, and 90° angles of bypass graft, respectively. By comparing the results obtained from the model with no a bypass graft, it is noted that the blood velocity tends to decrease in magnitude in the model with a bypass graft. The results also indicate that the flow from the stenosed artery becomes a jet flow when interacting with the flow from the graft. When it arrives to the heel, it hits the flow from the graft. This reduces the magnitude of blood velocity near the graft region.

To demonstrate the characteristics of blood pressure and velocity in the stenosed artery, in Figures 6 and 7, we show the pressure distribution along the arterial axis and the velocity distribution along the radial axis at the throat during the systolic and diastolic periods. The arterial axis and the radial axis along which results are examined are shown in Figure 5(a). The instants of time for which results are presented are shown in Figure 5(b). The results of Figures 6 and 7 show that the pressure drops very fast around the stenosis site for any bypass graft angles, and it produces high blood velocity in this region.

Figures 8 and 9 show the velocity distribution in the heel and toe parts and the far distal part in five cardiac cycles. In Figures 8, the jet flow from the host artery decreases when the 45° angle bypass operation is used in the model. In the model with no bypass operation, the velocity in the far distal part is very low compared to the one with the bypass operation. In the model with no bypass graft,

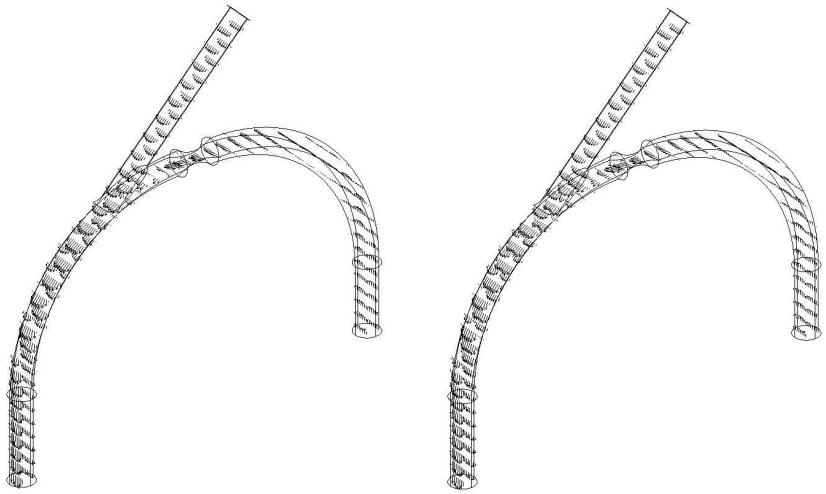

(a) (b)

FIGURE 3. The velocity profile in RCA at two different instants of time during a cardiac cycle: (a) at the peak of systole $t = 0.25s$, (b) at the peak of diastole $t = 0.5s$.

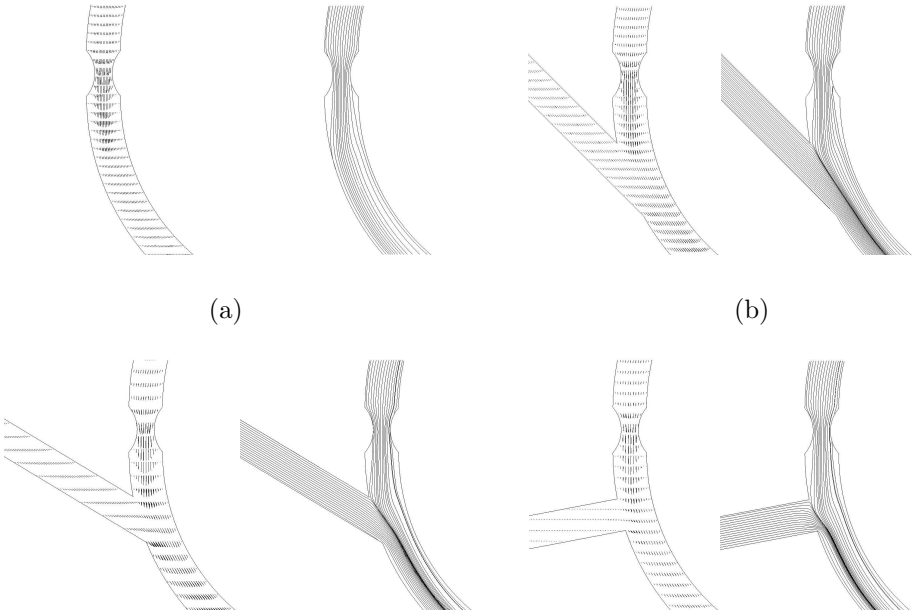

(a) (b)

(c) (d)

FIGURE 4. The velocity vectors and the streamlines of blood flow in the right coronary artery on the x-z plane at the instant of time $t = 0.1$s (beginning of the systole): (a) with no bypass, and (b)-(d) with bypass operation 45°, 60°, and 90°, respectively.

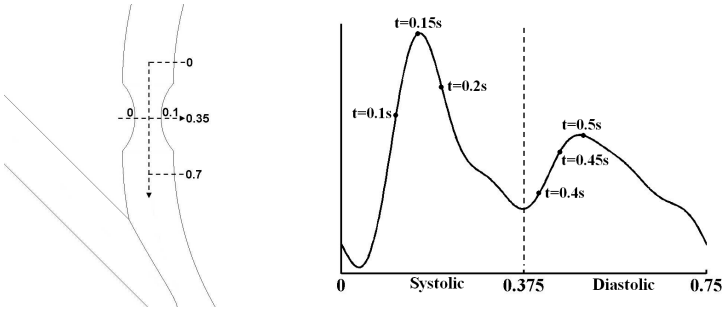

(a) (b)

FIGURE 5. (a) The arterial axis and the radial axis along which results are examined, (b) the instants of time during a typical cardiac cycle for which results are presented.

the maximum blood speed in the far distal part is equal to 40.41 cm/s. However, when we use the 45°, 60°, and 90° angles of bypass graft, blood speed in the far distal part tends to increase and reaches 78.08, 70.91, and 54.07 cm/s, respectively. In addition, the maximum blood speed in the far distal part decreases as the angle of bypass graft increases.

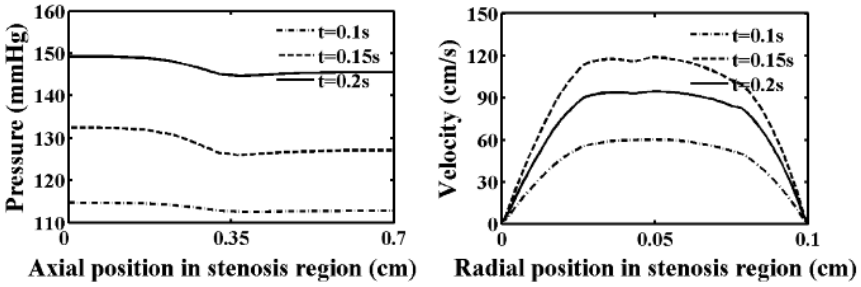

(a)

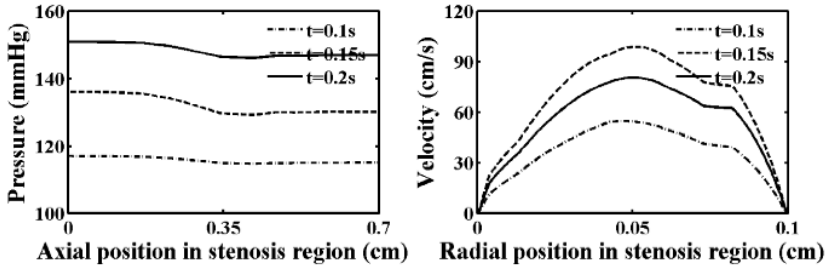

(b)

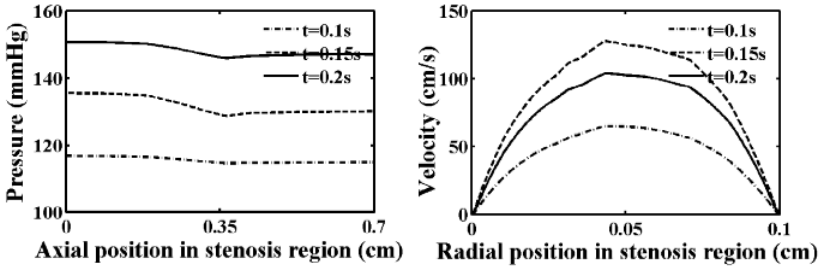

(c)

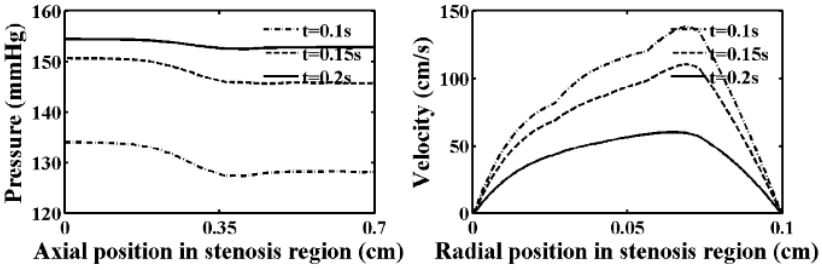

(d)

FIGURE 6. The distributions of pressure and velocity in the stenosis region at the systole period: (a) with no bypass graft, (b)-(d) with bypass graft angles 45°, 60°, and 90°, respectively. (The stenosis is located at 0.35.)

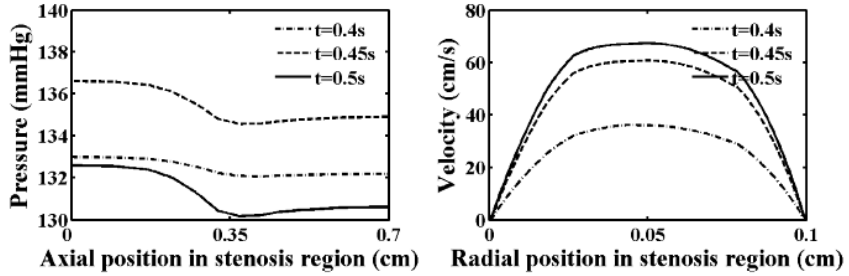

(a)

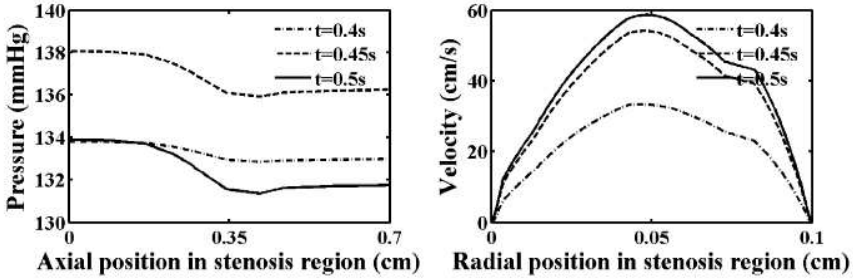

(b)

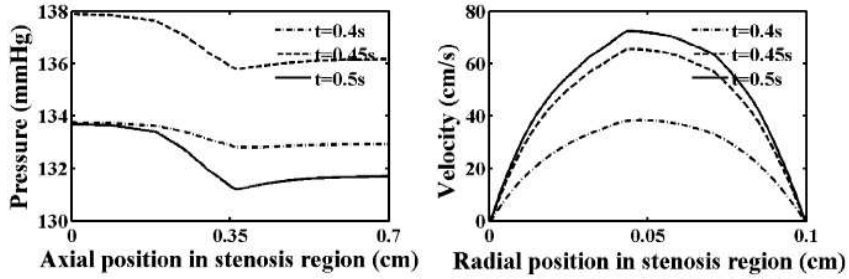

(c)

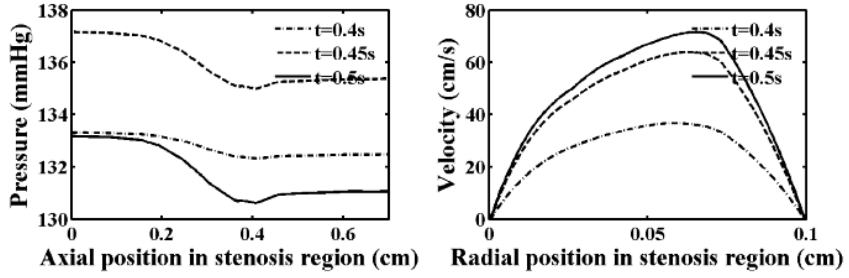

(d)

FIGURE 7. The distributions of pressure and velocity in the stenosis region at the diastole period: (a) with no bypass graft, (b)-(d) with bypass graft angles 45°, 60°, and 90°, respectively.

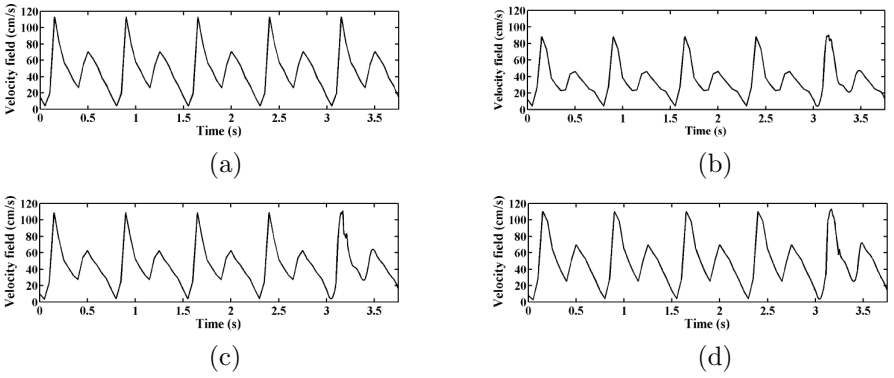

FIGURE 8. The distribution of velocity in the heel and toe parts (C) (see Figure 2(b)): (a) with no bypass graft, (b)-(d) with bypass graft angles 45°, 60°, and 90°, respectively.

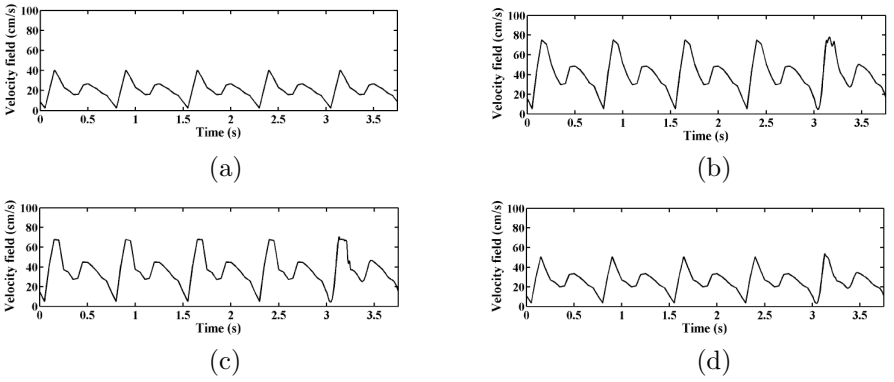

FIGURE 9. The distribution of velocity in the far distal part (D): (a) with no bypass graft, (b)-(d) with bypass graft angles 45°, 60°, and 90°, respectively.

To determine the critical flow condition, it is necessary to predict the wall shear stress. Thus, we plot the wall shear stress along the bed of the host artery in Figure 10 to show the influence of bypass graft. The results indicate that the magnitude of wall shear stress varies between 0 and 4150 dyn/cm^2 and high negative wall shear stress occurs around the stenosis site.

5. **Conclusions.** This study is undertaken to provide a better understanding of the bypass graft effects on blood flow through a 75% stenosed right coronary artery. The model is presented based on a non-Newtonian model and the Bubnov-Galerkin finite element formulation. The use of the pulsatile velocity at the inlet and the pulse pressure at the outlet is aimed to simulate the real blood flow. Comparing the results for different angles of bypass grafts, the one with a 45° graft angle seems to perform better. However, the results illustrate that the low wall shear stress in the bed of the stenosed artery and the negative value of shear stress in the stenosis region may indicate that atherosclerotic lessions will develop. In addition to the

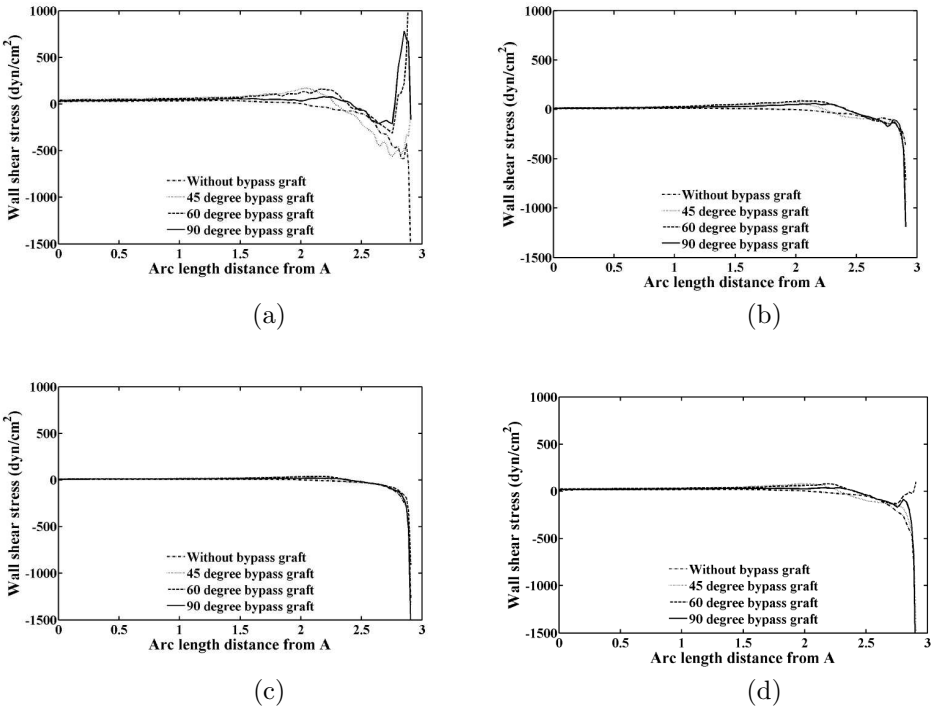

FIGURE 10. The distribution of wall shear stresses along the bed of artery (along the line from A to A′; see Figure 1(b)) at various instants: (a) t=0.15s, (b) t=0.25s, (c) t=0.35s, and (d) t=0.5s. (The stenosis is at a distance 2.5 cm from A.)

effects on the flow patterns demonstrated here, other mechanisms may affect the formation of atherosclerosis. It is noted that the proper choice of the diameter of the graft might improve the balance of inflow and outflow in the coronary artery. We should also emphasise that to improve the accuracy of results, the effect of porous wall and wall deformation must be included. Therefore, further research will be carried out to include the effect of wall deformation.

Acknowledgments. The authors are grateful to the Commission on Higher Education Staff Development Project Scholarship, the Thailand Research Fund (TRF), and the 2005 Australia Endeavour Chueng Kong Awards for supporting this research and also wish to thank the Division of Cardiac Surgery, Heart Institute, Saint Louis Hospital and Foundation for providing some of the data for the analysis. The authors are also grateful to the referees, whose comments led to a number of significant improvements.

REFERENCES

[1] Organisation Mondiale de la Santé (OMS). Annual Report, 1999.
[2] C.R. Ethier, D.A. Steinman, X. Zhang, S.R. Karpik, M. Ojha, FLOW WAVEFORM EFECTS ON END-TO-SIDE ANASTOMOTIC PATTERNS. J Biomech 31(1998) 609-17.
[3] J. Hun, W. C. Jong, G.P. Chan, ASYMMETRIC FLOWS OF NON-NEWTONIAN FLUIDS IN SYMMETRIC STENOSED ARTERY. Korea-Australia Rheology Journal 16(2004) 101-8.

[4] M. Lie, D. P. Giddens, S. A. Jones, F. Loth, H. Bassiouny, Pulsatile flow in an end-to-side vascular graft model: Comparison of computations with experimental data. J Biomech Eng 123(2001) 80-7.
[5] D. Tang, C. Yang, S. Kobayashi, D.N. Ku, Steady flow and wall compression in stenotic arteries: A three-dimensional thick-wall model with fluid-wall interactions. J Biomech Eng 123(2001) 548-57.
[6] M. Bonert, J. G. Myers, S. Fremes, J. Williams, C. R. Ethier, A numerical study of blood flow in coronary artery bypass graft side-to-side anastomoses. Ann Biomed Eng 30(2002) 599-611.
[7] Y. Papaharilaou, D.J. Doorly, S.J. Sherwin, The influence of out-of-plane geometry on pulsatile flow within a distal end-to-side anastomosis. J Biomech 35(2002) 1225-39.
[8] E.S. Weydahl, J.M. Moore Jr., Dynamic curvature strongly affects wall shear rates in a coronary artery bifurcation model. J Biomech 34(2001) 1189-96.
[9] D.N Ku, Blood flow in arteries. Annu Rev Fluid Mech 29(1997) 399-434.
[10] B. Berthier, R. Bouzerar, C. Legallais, Blood flow patterns in an anatomically realistic coronary vessel: Influence of three different reconstruction methods. J Biomech 35(2002) 1347-56.
[11] Y.I. Cho, K.R. Kensey, Effects of the non-Newtonian viscosity of blood on flows in a diseased arterial vessel. Part 1: Steady flows. Biorheology 28(1991) 241-62.
[12] C. Bertolotti, V. Deplano, J. Fuseri, P. Dupouy, Numerical and experimental models of post-operative realistic flows in stenosed coronary bypasses. J Biomech 34(2001) 1049-64.
[13] A. Quarteroni, L. Formaggia, Mathematical modelling and numerical simulation of the cardiovascular system, chapter in modelling of living systems, Handbook of Numerical Analysis Series, (P.G Ciarlet et J.L. Lions, Eds.), Elsevier, Amsterdam, 2004.
[14] B.M Johnston, P.R Johnstona, S. Corneyb, D. Kilpatrick, Non-Newtonian blood flow in human right coronary arteries: Steady state simulations. J Biomech 37(2004), 709-20.
[15] C. Jie, L. Xi-Yun, Numerical investigation of non-Newtonian blood flow in a bifurcation model with non-planar branch. J Biomech 37(2004) 1899-1911.
[16] F.J.H Gijsen, F.N van de Vosse, J.D. Janssen, The influence of the non-Newtonian properties of blood on the flow in large arteries: Steady flow in a carotid bifurcation model. J Biomech 32(1999) 601-8.
[17] D.Y. Fei, J.D. Thomas, S.E. Rittgers, The effect of angle and flow rate upon hemodynamics in distal vascular graft anatomoses: A numerical model study. J Biomech Eng 116(1994) 331-6.
[18] M-H. Song, M. Sato, Y. Ueda, Three-dimensional simulation of coronary artery bypass grafting with the use of computational fluid dynamics. Surg Today 30(2000) 993-8.
[19] C. Bertolotti, V. Deplano, Three-dimensional numerical simulations of flow through a stenosed coronary bypass. J Biomech 33(2000) 1011-22.
[20] T. Ishikawa, L. F. R. Guimaraes, S. Oshima, R. Yamane, Effect of non-Newtonian property of blood on flow through a stenosed tube. Fluid Dynamics Research 22(1998) 251-64.
[21] S. A. Berger, L-D. Jou, Flows in stenotic vessels. Annu. Rev. Fluid Mech 32(2000) 347-82.

Received on December 6, 2005. Accepted on January 26, 2006.

E-mail address: scbww@mahidol.ac.th
E-mail address: dpoltem@yahoo.com
E-mail address: yhwu@maths.curtin.edu.au
E-mail address: scylb@mahidol.ac.th